Sideband Harmonic-Based Talkative Power Conversion

Zewen Wang, *Student Member, IEEE*, Dehong Zhou, *Senior Member, IEEE*, Xin Liu, *Member, IEEE*, Zewei Shen, *Member, IEEE*, and Jianxiao Zou, *Member, IEEE*

***Abstract*—Talkative power conversion (TPC) is a promising solution to modern power system communication due to its advanced features of reduced communication infrastructure and low volume. However, the majority of TPC in three-phase inverters is realized by superimposing the frequency-hopping sinusoidal reference signals, which adversely affects the power quality and stability from the perspective of the power system. In view of this, this article proposed a sideband harmonic-based TPC scheme for three-phase inverters without extra harmonics injection. In the proposed scheme, the signal is modulated into the carrier-based pulsewidth modulation by binary phase-shift keying modulation and is transmitted over power lines via sideband harmonics. Sideband harmonics with different carrier phases are analyzed by double Fourier series (DFS) and modeled under *dq* frame for efficient demodulation. The proposed strategy takes advantage of the existing sideband harmonics to achieve TPC in three-phase inverters, which avoids introducing extra harmonics and has less impact on the power quality. As a result, the given solution not only reduces system costs and volume but also realizes a power quality-friendly signal transmission. Finally, the feasibility of the proposed TPC method is verified by the experimental platform.**

***Index Terms*—AC power systems, carrier-based pulsewidth modulation (CBPWM), sideband harmonics, talkative power conversion (TPC), three-phase inverters.**

Manuscript received 6 January 2024; revised 8 May 2024; accepted 12 June 2024. Date of publication 17 June 2024; date of current version 4 September 2024. This work was supported in part by the National Natural Science Foundation of China under Grant 62173067, in part by the Guangdong Basic and Applied Basic Research Foundation under Grant 2024A1515010184, and Grant 2023A1515240060, in part by the Guangdong Science and Technology Program under Grant 2021QN02L854, Sichuan Science and Technology Program under Grant 2023NSFSC0298, and in part by the Shenzhen Science and Technology Program under Grant JCYJ20220530165001003, Grant JCYJ 20230807120006012, and Grant JSGG20220831110805010. Recommended for publication by Associate Editor L. Zhang. *(Corresponding author: Dehong Zhou.)*

Zewen Wang, Xin Liu, and Jianxiao Zou are with the Shenzhen Institute for Advanced Study, University of Electronic Science and Technology of China, Shenzhen 518000, China (e-mail: 202222280546@std.uestc.edu.cn; liu_xin@uestc.edu.cn; jxzou@uestc.edu.cn).

Dehong Zhou is with the School of Automation Engineering, University of Electronic Science and Technology of China, Chengdu 611731, China, and also with the Shenzhen Institute for Advance Study, University of Electronic Science and Technology of China, Shenzhen 518000, China (e-mail: dhzhou@uestc.edu.cn).

Zewei Shen is with the School of Automation Engineering, University of Electronic Science and Technology of China, Chengdu 611731, China (e-mail: shenzw@uestc.edu.cn).

Color versions of one or more figures in this article are available at https://doi.org/10.1109/TPEL.2024.3415425.

Digital Object Identifier 10.1109/TPEL.2024.3415425

I. Introduction

DUE to the rising global energy expenditure costs and huge electricity demand, a growing number of distributed energy resources (DERs) have been connected to modern power systems, such as wind turbines [1], photovoltaic plants [2], and energy storage systems [3]. However, the increasing presence of DERs could generate some critical situations, such as grid instability and unwanted equipment failure, which pose brand-new challenges to the stable operation of the power system [4]. The rapid growth of DERs has prompted increasing interest in the monitoring and control of DERs through smart grid communications [5]. Information and communication technology is recognized as a promising solution for the efficient and intelligent performance of power systems [6]. Hence, it is becoming necessary to enhance communication and information transmission technology for ever-increasing DERs to achieve better device monitoring and real-time control.

Communication in power systems is mainly realized by wireless communication, wired communication, and power line communication (PLC). Wireless communication has good characteristics of adaptability and rapidity, but its transmission distance is limited due to signal attenuation. Moreover, it is also threatened by noises and cyber-attacks [7]. Unlike wireless communication, wired communication has the advantages of strong anti-interference and low attenuation. However, using additional communication lines would bring high costs of installation and maintenance [8]. By utilizing the existing power system as a medium for signal transmission, PLC avoids the use of standalone communication systems and has good communication stability. Nevertheless, conventional PLC requires additional circuits for injecting and amplifying sinusoidal signals at a specific frequency, which increases the grid system cost and reduces the efficiency of the system's energy transmission [9], [10]. Therefore, a reliable and economical communication technology is urgently needed for modern power system signal transmission.

In recent years, the study of power electronics technology elucidates that power electronic converters are capable of transmitting information and can avoid the abovementioned disadvantages in conventional PLC [11], providing a novel communication method for modern power systems. Fig. 1 shows the application of the converter in the power system. As an interface device, power electronic converters are widely used to connect DERs to the power grid. In the process of electric power conversion, power electronic converters act as active

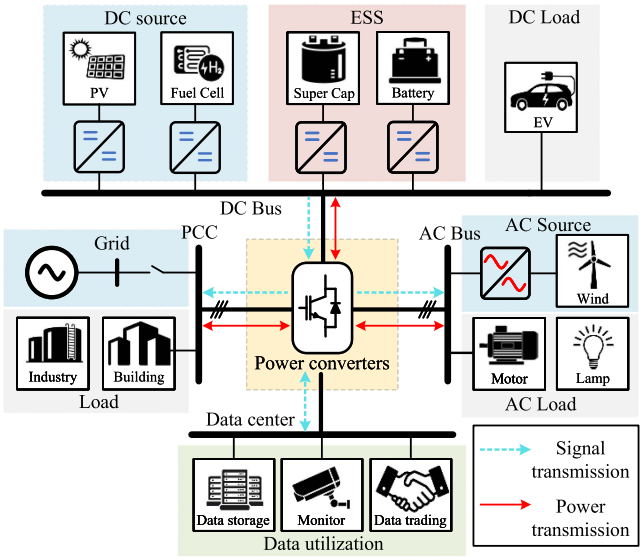

Fig. 1. Power converters used for energy conversion and communication in power system.

devices that can encode as well as signalize, bringing additional degrees of freedom for communication in the power system. The approach of using power electronic converters for signal transmission is called talkative power conversion (TPC) and has been investigated these years [12]. TPC takes advantage of the direct connection and encoding ability of the power converters, which avoids additional coupling circuits and enables efficient information transfer.

As an innovative communication technology, TPC is favored by many experts and scholars. The literature [13] and [14] utilize the Buck converter with a multipath load structure to realize the signal transmission function while converting power. Signals are embedded into the switching frequency with the pulsewidth modulation (PWM) technique, and the switching ripple generated from the converters can carry information. The literature [12] studies the essential nature of converters and characterizes the similarity of operation principle to that of communication systems, in which TPC is first proposed from the view of power conversion and communication. Up to now, TPC has been researched and applied to battery management systems [15], switching reluctance generators [6], [16], [17], wireless charging for electric vehicles [18], and visible light communication [11], [19]. Compared with the conventional PLC methods, TPC realizes efficient information transmission and contributes to reduced system complexity, cost, and volume [20]. However, these methods fit exclusively for particular dc–dc converter configurations and little work related to TPC in dc–ac inverters has been conducted due to the complexity of harmonic components and disturbance in the ac grid.

As one of the most employed power converters for energy transformation, three-phase inverters with TPC have great research value and wide application prospects. The literature [21] uses the primary control loop and the modulation of the power converter for sending and receiving data. The proposed method injects the information-carried fractional harmonicas as current references to the current loops, where the primary control loop and the modulation of the inverters are used for sending and receiving data. In [22], the small-signal model of the three-phase voltage source inverter is discussed to analyze the stability after injecting the signal and verify the feasibility of the inverter-based TPC system. However, it should be noted that stability problems may be caused at higher frequencies due to voltage or current superposition. Another TPC method by changing the parameters of the PWM carrier signal is given in [23]. By using frequency-shift keying (FSK) modulation, the signal can be embedded in the PWM carrier and then injected into the output voltage ripples. However, it is noticeable that the switching frequency variation will cause data-dependent ripple fluctuations in converters [24]. From a power system point of view, TPC-FSK would result in power quality issues [25]. Accordingly, TPC methods mentioned above in ac power systems do not take power quality and system stability into account, which is an urgent issue to be addressed.

In view of this, a novel TPC method for three-phase inverters is proposed in this article. The main contributions of this article are listed as follows.

1) A sideband harmonic-based TPC method for three-phase inverters is first proposed in this article. The information is modulated into the voltage sideband harmonics by changing the phase of the PWM carrier and transmitted on the power line without extra coupling devices.
2) By analyzing the mathematical model of carrier-based PWM (CBPWM) harmonics in the dq-axis, the abc-dq coordinate transformation is chosen to suppress carrier harmonics and increase the signal demodulation rate.
3) The proposed sideband harmonic-based TPC strategy does not require additional harmonic injection, which has a low impact on power quality with total harmonic distortion (THD) fluctuations below 0.1%.
4) In response to the frequency domain characteristics of sideband harmonics, this article designs a two-step coherent demodulation to quickly and accurately demodulate the signal-carried harmonics.

The rest of this article is organized as follows. In Section II, the basic concepts of TPC are given and the three-phase inverter harmonic spectrum is analyzed by Fourier transform. In Section III, the implementation of TPC in three-phase inverters is shown, including signal modulation, signal transmission medium selection, and signal demodulation. The experimental results and TPC implementation process are provided in Section IV. Finally, Section V concludes this article.

II. Basic Concept of TPC and Harmonic Analysis

In this section, the basic concepts of TPC are introduced. TPC is defined as the combination of power electronic technology and communication technology for modern power system signal transmission. Due to the characteristics of TPC, the analysis of harmonic components in the output voltage is delicately given. The harmonic spectrum in the output voltage is delicately analyzed by double Fourier transform. After mathematically manipulating the formulation and comparison, the amplitude,

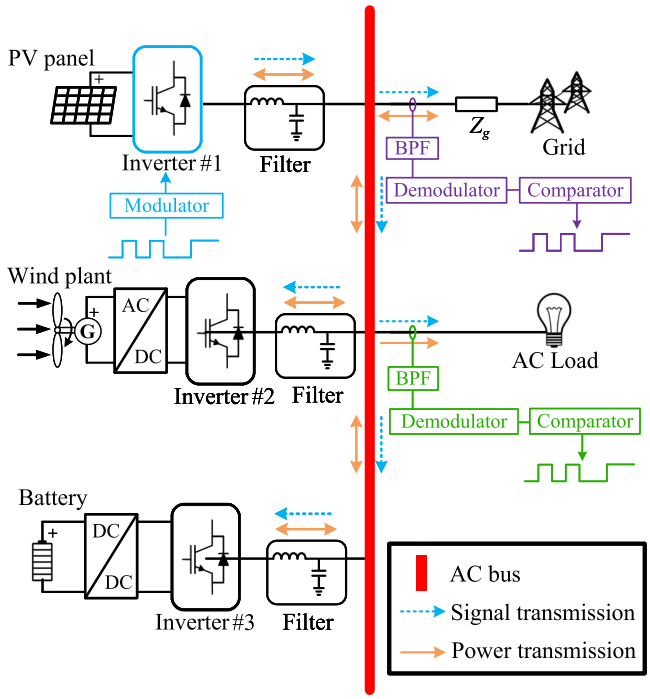

Fig. 2. Schematic diagram of the inverter-based power and information network.

frequency, and phase are the appropriate medium for signal modulation in the TPC.

A. Implementation of TPC in Inverter and AC Power System

Power electronic technology performs a controlled transformation of electrical energy, before and after which the electrical energy is in analog form. However, due to the switching mode of operation, there is a discrete intermediate process in the power conversion process, which is qualitatively different from the traditional power processing method. In the process of power conversion and control, the power converter first converts the analog input power into discrete power pulses, then passes through a filter to obtain the analog output power. During the power discretization, the discrete power pulse sequence has the ability to be encoded and loaded with digital information, thus, has the potential for information transmission. TPC takes advantage of the codable property of power converters to couple the signal to the power line in the form of voltage ripples, which enables the simultaneous transmission of power and signal.

As one of the most used power converters in ac power systems, inverters connect multiple DERs to power distribution systems effectively [26]. The schematic of the inverter-based power system is illustrated in Fig. 2, where renewable energy sources and ESSs are connected to ac bus by inverters. In the process of electrical energy conversion, inverters act as active devices and can be coded in the process of electrical energy conversion, which provides additional degrees of freedom for communication in the power grid. The role as the interface between different electrical domains and the capability of active coding make inverters an ideal and potential channel for TPC in ac power systems.

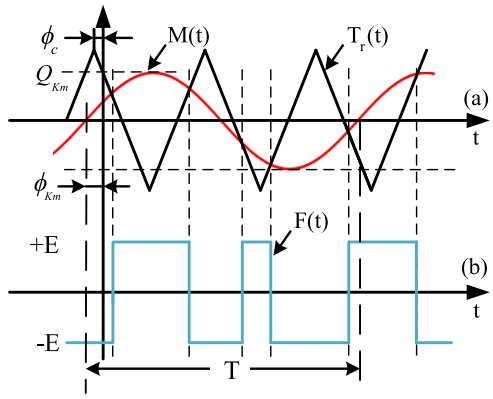

Fig. 3. CBPWM in inverters. (a) Triangular wave modulation of CBPWM. (b) CBPWM output driving signals.

B. Analysis of Harmonic Generated by CBPWM in Three-Phase Inverters

During the process of power conversion, the inverter transforms the amplitude, polarity, and impedance of the electrical energy, and the most common power control method is using CBPWM. Compared with the harmonic spectrum generated from dc–dc converters, the harmonic spectrum of CBPWM is more complicated in three-phase inverters. Moreover, when the digital control is employed, the sampling and hold procedure also introduces sideband components [27]. As the principle of TPC is to use the output voltage harmonics for signal transmission, understanding the relevant characteristics of the harmonics is better for designing filters and demodulation. Therefore, the employed harmonics would be first analyzed and discussed mathematically.

Fig. 3 shows the principle of natural sampling bipolar CBPWM. In the figure, $M(t)$ is the sinusoidal reference signal and $T_r(t)$ is the triangular carrier signal. The expression for the sinusoidal reference signal $M(t)$ in Fig. 3(a) is as follows:

$$M(t) = Q_{Km} cos(\omega_0 t + \phi_{Km}),$$
$$Q_{Km} = \frac{M_c \pi}{2}, M_c < 1 \quad (1)$$

where Q_{Km}, ω_0, ϕ_{Km} and M_c are the amplitude, angular frequency, initial phase angle, and modulation index of the sinusoidal reference signal $M(t)$. When the sinusoidal reference signal is larger than the triangular carrier signal, the output signal $F(t)$ is at a high level; otherwise, $F(t)$ is at a low level. Fig. 3(b) shows the CBPWM output waveform, whose maximum magnitude is E.

Double Fourier series (DFS) expansion is a well-established approach commonly used for the frequency-domain representation of the CBPWM waveform with a single-frequency sinusoidal modulation signal, and has been extensively applied in inverters for analyzing the complex harmonics [28]. DFS treats the CBPWM waveform as a stationary signal in two dimensions, which correspond to the carrier frequency and the frequency of the modulating wave, respectively [29]. With DFS expansion, the components of each harmonic can be calculated

accordingly [30]. The DFS expression can be written as follows:

$$f(x,y)=\frac{A_{00}}{2}+\sum_{n=1}^{\infty}\{A_{0n}\cos ny+B_{0n}\sin ny\}+\sum_{m=1}^{\infty}\{A_{m0}\cos mx+B_{m0}\sin mx\}+\sum_{m=1}^{\infty}\sum_{\substack{n=-\infty\\(n\neq 0)}}^{\infty}\begin{Bmatrix}A_{mn}\cos(mx+ny)\\+B_{mn}\sin(mx+ny)\end{Bmatrix} \tag{2}$$

$$C_{mn}=A_{mn}+jB_{mn}=\frac{1}{2\pi^2}\int_{-\pi}^{\pi}\int_{-\pi}^{\pi}f(x,y)e^{j(mx+ny)}dxdy \tag{3}$$

where m is the carrier index variable, n is the baseband index variable, $x(t)=\omega_c t+\phi_c$, $y(t)=\omega_0 t+\phi_{Km}$, ω_c and ϕ_c are the carrier angular frequency and carrier phase, respectively. $|C_{mn}|$ can be seen as the amplitude of each harmonic.

Through the DFS expansion of the CBPWM signal, the amplitude, frequency, and phase of each harmonic can be obtained [31]. The mathematical model of output phase voltage u_o in terms of DFS is written as follows:

$$u_o=\frac{2Q_{Km}E}{\pi}\cos(\omega_0 t+\phi_{Km})+\sum_{m=1}^{\infty}\left(\frac{4E}{m\pi}\right)J_0(mQ_{Km})\sin\left(\frac{m\pi}{2}\right)\cos[m(\omega_c t+\phi_c)]+\sum_{m=1}^{\infty}\sum_{n=-\infty}^{+\infty}\left(\frac{4E}{m\pi}\right)J_n(mQ_{Km})\sin\left(\frac{m+n}{2}\pi\right)\cdot\cos[m(\omega_c t+\phi_c)+n(\omega_0 t+\phi_{Km})] \tag{4}$$

where J_0 is the 0-order Bessel function and J_n is the n-order Bessel function. The characteristic of the Bessel Function is also given

$$J_n(x)=\sum_{m=0}^{\infty}\frac{(-1)^m}{m!\Gamma(m+n+1)}\left(\frac{x}{2}\right)^{2m+n} \tag{5}$$

$$J_{-n}(x)=(-1)^n J_n(x). \tag{6}$$

In the three-phase inverter system, there exists a 120° phase difference between adjacent voltages. Therefore, if the initial phase angle in phase A is ϕ_{Km}, then the angles of phases B and C will be ($\phi_{Km}-2\pi/3$) and ($\phi_{Km}+2\pi/3$), respectively.

Fig. 4(a) shows the harmonic spectrum in the inverter CBPWM output phase voltage. The phase voltage can be divided into three parts according to (4): fundamental component, carrier harmonics, and sideband harmonics. It is obvious that the parameters (frequency, phase, amplitude) in the reference voltage signal are mapped to the baseband signal and sideband harmonics, while the carrier signal parameters are loaded into the carrier harmonics and sideband harmonics. By changing the parameters of the CBPWM signals, the voltage harmonics in the output voltage are indirectly affected, and these harmonics convey the changes as they are transmitted over the power line,

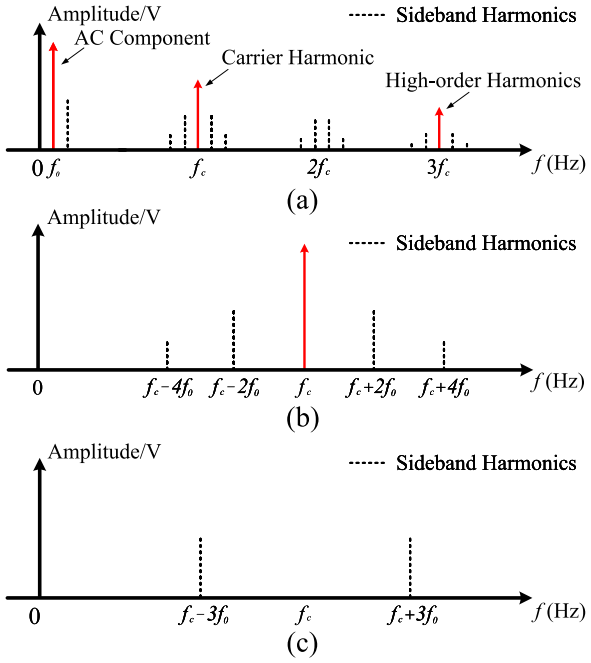

Fig. 4. Analysis of harmonics in the CBPWM output voltage. (a) Harmonics components in the phase voltage. (b) Carrier harmonic and sideband harmonics when $m=1$ in phase voltage. (c) Carrier harmonic and sideband harmonics when $m=1$ in d-axis voltage.

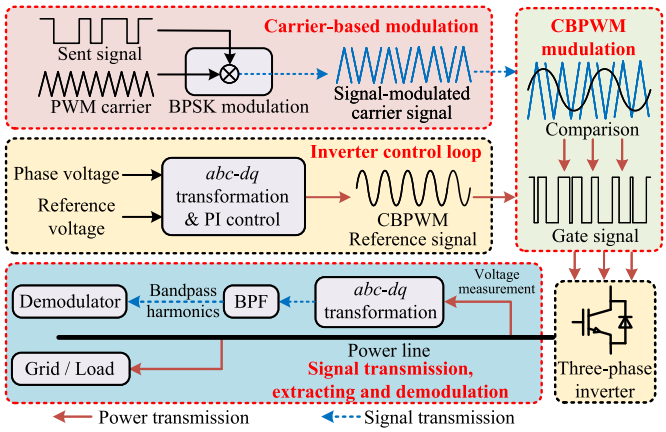

Fig. 5. Diagram of the proposed TPC strategy.

which not only avoids additional coupling devices and communication lines but also achieves effective signal synchronous transmission on the power line.

III. Sideband Harmonics-Based TPC Scheme

In this section, the principle of signal modulation and demodulation is introduced to realize TPC. The diagram of TPC is shown in Fig. 5. In Fig. 5, the sideband harmonic-based TPC scheme can be divided into the following three parts: signal modulation, sideband harmonic transmission, and information-carried sideband harmonic demodulation. The signal injection is an important part of the proposal. From the view of the power system, the TPC strategy is supposed to be friendly to

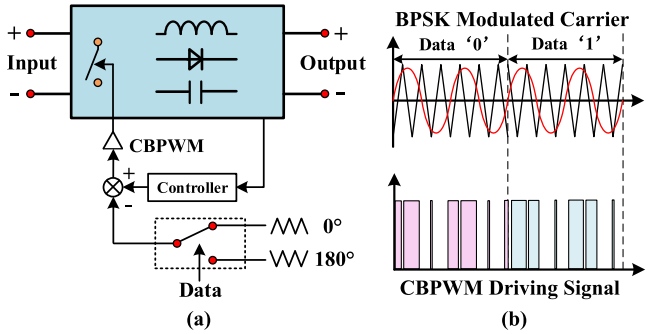

Fig. 6. Modulation in inverters. (a) Signal modulated into the CBPWM carrier by BPSK. (b) Phase changes in CBPWM driving signal.

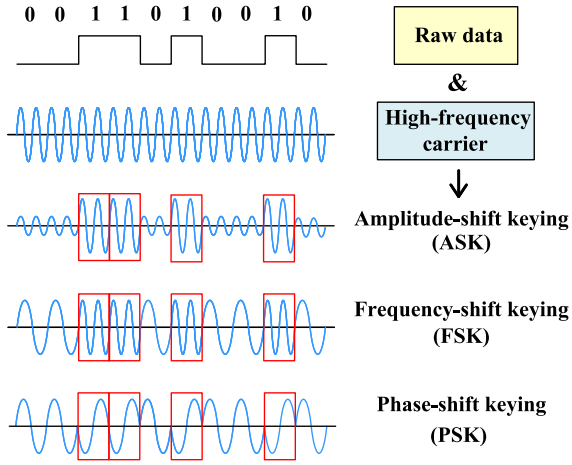

Fig. 7. Comparison of three commonly used modulation.

the power quality. Given this, the method of modulation and carrier for signal are highlighted in this section. According to the modulation method and characteristics of sideband harmonics, the signal transmission and demodulation can also be solved.

A. Principle of CBPWM Signal Modulation

As noted earlier, harmonics generated from CBPWM are affected by the CBPWM reference signals and carrier signals. By changing one or several freedom degrees (amplitude, frequency, phase) of the CBPWM signals (reference or carrier signals), the information can be loaded to the inverter output harmonics for transmission without coupler hardware. The process of freedom degree variation is called CBPWM signal modulation. Depending on the medium in which the signal is modulated, it can be categorized into reference-signal-based (RS) modulation and carrier-signal-based (CS) modulation [24]. RS modulation superimposes the information on the reference voltage, whereas CS modulation changes the carrier in the modulation process. In contrast to RS modulation, CS modulation does not require additional reference voltage or current injections, which is more reliable and power quality-friendly. The result of CS modulation will be reflected in the inverter output harmonics shown in (4). In view of this, CS modulation is adopted to achieve TPC in this article.

Fig. 6 shows how the signals are embedded into the CBPWM triangular carrier in the three-phase inverter. The CS modulation technique here focuses on the switching mode of operation of the inverter, utilizing discrete transition states during the power conversion process to load signals onto discrete power pulses, which in turn are reflected in the switching ripples of the power outputs. As a result, the sent signals achieve the conversion from digital baseband signals to digital bandpass signals.

B. Digital Signal Modulation

Digital signal modulation implements the conversion of digital baseband signals to digital bandpass signals, which is used to modulate the digital signal onto the CBPWM carrier signal in CS modulation. Common digital signal modulation techniques are shown in Fig. 7, which include amplitude-shift keying (ASK) modulation, FSK modulation, and phase-shift keying (PSK) modulation. These modulation methods correspond to the three variable degrees of freedom in output harmonics, thus all of them can be used in TPC.

According to (4), using ASK in the CBPWM carrier would change the amplitude of the carrier harmonics and the sideband harmonics, which may affect the output voltage power quality. Similarly, frequent changes in CBPWM carrier will lead to signal-related ripple reflections in the power converter, also resulting in power quality problems from the point of view of the power system [24]. PSK in CS modulation is based on varying the CBPWM carrier phase angle, given a fixed carrier amplitude and a fixed carrier frequency. Compared with ASK and FSK, taking PSK modulation can avoid power quality problems caused by changes in output harmonics and is effective in saving bandwidth. In view of this, PSK is chosen as the modulation method for TPC in this article.

For any signal $f(x)$ with period T and angular frequency $\omega = 2\pi/T$, its Fourier series expansion can be expressed as

$$F(x) = \frac{1}{2}a_0 + \sum_{n=1}^{\infty}(a_n \cos n\omega x + b_n \sin n\omega x) \tag{7}$$

where the coefficients a_0, a_n, and b_n in this series are defined by

$$\begin{aligned} a_0 &= \tfrac{2}{T}\textstyle\int_{-T/2}^{T/2} f(x)dx \\ a_n &= \tfrac{2}{T}\textstyle\int_{-T/2}^{T/2} f(x)\cos n\omega x dx \\ b_n &= \tfrac{2}{T}\textstyle\int_{-T/2}^{T/2} f(x)\sin n\omega x dx. \end{aligned} \tag{8}$$

In PSK, M signal waveforms can be derived as follows:

$$\begin{aligned} s_m(t) &= \mathrm{Re}\left[g(t)\mathrm{e}^{\mathrm{j}2\pi k/M}\mathrm{e}^{\mathrm{j}2\pi f_c t}\right] \\ &= g(t)\cos\left(2\pi f_c t + \frac{2\pi k}{M}\right) \\ k &= 0, 1, \cdots, M-1, 0 \le t \le T \end{aligned} \tag{9}$$

where $g(t)$ is the signal pulse function, $f_c = \omega_c/2\pi$ is the frequency of the carrier and $\theta_k = 2\pi k/M$ is the M kinds of possible phases of the carrier. In binary PSK (BPSK), $M = 2$ and the initial phase of 0° and 180° are used to represent bit "0"

and bit "1," respectively. These signal waveforms have equal energy and can be represented as

$$E_{\mathrm{s}} = \int_0^T s_m^2(t)\mathrm{d}t = \frac{1}{2}\int_0^T g^2(t)\mathrm{d}t = \frac{1}{2}E_{\mathrm{g}}. \tag{10}$$

When $g(t)$ is a square wave, it can be expressed as

$$s_m(t) = \sqrt{\frac{2}{T}}\cos\left(2\pi f_{\mathrm{c}}t + \frac{2\pi k}{M}\right). \tag{11}$$

At this point, the transmitted signal has an invariant envelope, while the carrier phase begins to change at each symbol interval

$$\begin{aligned} s_m(t) &= s_{m1}\phi_1(t) + s_{m2}(t)\phi_2(t) \\ \phi_1(t) &= \sqrt{\frac{2}{E_g}}g(t)\cos\left(2\pi f_c t\right) \\ \phi_2(t) &= \sqrt{\frac{2}{E_g}}g(t)\sin\left(2\pi f_c t\right). \end{aligned} \tag{12}$$

The two-dimensional vector $s_m = [s_{m1}, s_{m2}]$ can be written as

$$s_m = \left[\sqrt{\frac{E_g}{2}}\cos\frac{2\pi k}{M}, \sqrt{\frac{E_g}{2}}\sin\frac{2\pi k}{M}\right]. \tag{13}$$

Thus, the phase-modulated signal can be viewed as two orthogonal carriers whose amplitude depends on the phase transmitted within each signal interval, which can provide higher spectral efficiency and anti-interference ability for TPC in inverters.

C. Sideband Harmonics-Based TPC

As mentioned in (4), the carrier harmonics and the sideband harmonics all carry the frequency and initial phase information from the CBPWM carrier, which can be the information medium for power/signal carrier modulation. Using carrier harmonics as the medium for communication is a good idea, but the influence of sideband harmonics cannot be negligible. Compared to carrier harmonics, carrier harmonics are less prevalent in the ac grid and potential carrier harmonic cancellation may occur between the phase legs [31]. In addition, notice that the carrier harmonics are the same in each phase leg, but the sideband harmonics have a 120° phase difference between adjacent phase legs. Thus, the carrier harmonics can be eliminated in the line-to-line voltage or by coordinate transformation, while sideband harmonics can still be retained. In this case, using sideband harmonics as the medium can avoid the influences of carrier harmonics, thus decreasing the computational complexity of demodulation.

According to (4), the amplitude of the harmonics would decrease with the order m increasing. The resultant main sideband harmonic components' frequencies are located near the first-order ($m = 1$) and second-order ($m = 2$) carrier frequencies [32]. Harmonic components with larger amplitude carry more energy and could be easier to access. Given this, using first-order sideband harmonics for signal demodulation is a better choice.

Sideband harmonics with even combinations of $m + n$ are eliminated within each phase leg by the $\sin([m+n]\pi/2)$ according to (4). Consequently, all odd sideband harmonics are eliminated in the first-order sideband harmonic group, which means the significant sideband harmonics in this carrier group will occur at frequencies of $\omega_c t \pm 2\omega_0 t$ and $\omega_c t \pm 4\omega_0 t$. Moreover, it is noticeable that $\sin[(m+n)\pi/2]$ always equals to $\sin[(m-n)\pi/2]$ in first-order sideband harmonic group, so this set of sideband harmonics $H_{m=1}$ can be written as the product of two cos functions

$$\begin{aligned} H_{m=1} &= \sum_{n=1}^{+\infty}\left(\frac{4E}{\pi}\right)J_n\left(Q_{Km}\right)\sin\left(\frac{1\pm n}{2}\pi\right) \\ &\quad\cdot\cos[\omega_c t + \phi_c \pm n(\omega_0 t + \phi_{Km})] \\ &= \sum_{n=1}^{+\infty}\left(\frac{8E}{\pi}\right)J_n\left(Q_{Km}\right)\sin\left(\frac{1+n}{2}\pi\right) \\ &\quad\cdot\cos(\omega_c t + \phi_c)\cos(n\omega_0 t + n\phi_{Km}) \end{aligned} \tag{14}$$

Note that the sideband harmonics obtained from the filter are gathered in groups, which would affect the demodulation results and increase the bit error rate. In view of this, it is necessary to determine a separate group of sideband harmonics used for demodulation. Due to the characteristic of the Bessel function $J_n(Q_{Km})$, sideband harmonics with smaller $|n|$ have larger amplitude [31]. By adjusting the value of Q_{Km} and using *abc-dq* transformation, the first-order sideband harmonics with $|n| > 2$ can be suppressed. Therefore, the BPF output waveform can be approximated as the first-order sideband harmonics with $|n| = 2$, which are selected as the signal transmission carrier and demodulation target in this paper.

It is worth noting that the coordinate transformation is a common means when analyzing the sideband harmonics in three-phase inverters [33]. The output harmonics of each phase can be converted to the *dq* frame by *abc-dq* transformation. The first-order sideband harmonic components with $|n| = 2$ after *abc-dq* transformation can be written as (15), shown at the bottom of the next page.As illustrated in Fig. 4(c), it is obvious that not only the carrier harmonics are eliminated with the coordinate transformation, but also the bandwidth of the target sideband harmonics in *d*-axis voltage is widened, which facilitates higher signal transmission and demodulation rate.

D. Signal Demodulation From Sideband Harmonics

According to (14) and (15), the structure of the information-carried sideband harmonics is analogous to the double-sideband suppressed carrier (DSB-SC) modulation. Double-sideband (DSB) modulation is a commonly used modulation method for communication, and DSB-SC concentrates all the information in the DSB signal by suppressing the carrier. The process of DSB modulation is shown in Fig. 8. The CBPWM modulation generates sideband harmonics and indirectly realizes DSB modulation during the sampling process. After suppressing the carrier harmonics, the sideband harmonics carry all the information in the reference and CBPWM carrier signal, which are natural signal transmission mediums for TPC in the ac power system. In view

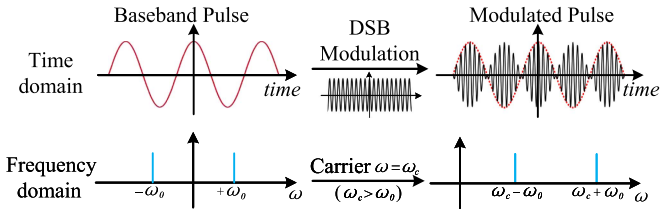

Fig. 8. DSB modulation in time and frequency domain.

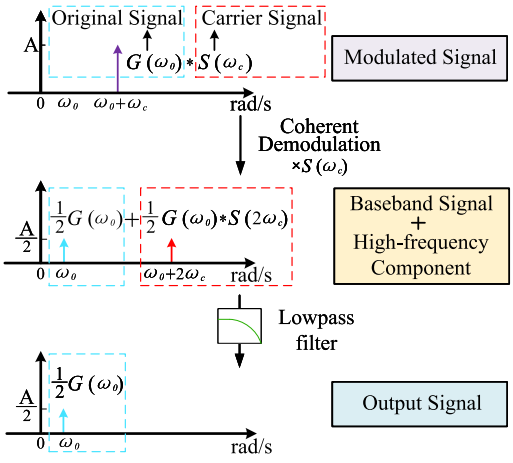

Fig. 9. Coherent demodulation in frequency domain.

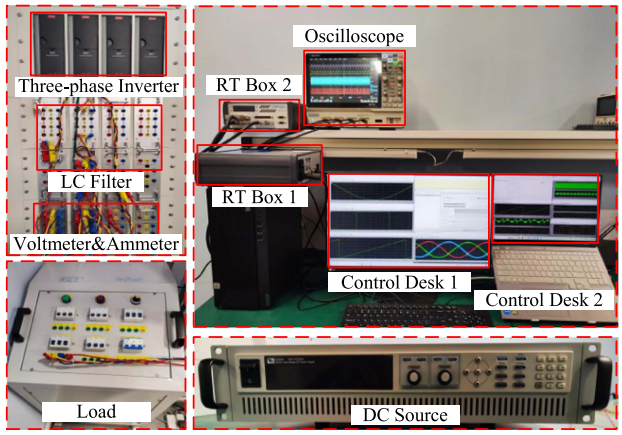

Fig. 10. Experimental test platform.

TABLE I
PARAMETERS OF THE PROTOTYPE SYSTEM

Parameter	Value
Rated dc voltage	270 V
Peak value of phase voltage	110 V
Switching frequency	10 kHz
Rated LC filter capacitor	3.5 μF
Rated LC filter inductance	2 mH
Output ac voltage frequency	50 Hz
Rated load resistance	44 Ω
Signal carrier amplitude	1 V
PLECS RT BOX 1/2 discrete sampling frequency	20 kHz

of this, the demodulation of the DSB harmonics can refer to the demodulation of DSB-SC.

Coherent demodulation is a classic method for BPSK and DSB demodulation. The steps and details of coherent demodulation are shown in Fig. 9. By providing a reference demodulation signal with the same frequency and phase as the sent signal, coherent demodulation enables fast and accurate signal demodulation for communication [34]. The key task is to realize phase and frequency synchronization for the demodulation signal. Common-used carrier synchronization methods include the phase-locked loop (PLL) and Costas loop [35]. The PLL technique is one of the most popular strategies for achieving frequency locking and is easy to implement. Thus PLL is used for synchronous demodulation signal generation in this article [36]. When there is no sent signal in the power line (sending bit "0"), PLL uses the output sideband harmonics of the BPF to control the frequency and phase of the oscillating signal inside the loop. The frequency and phase information of the oscillating signal in the ring is utilized to generate a fixed synchronous demodulated signal for subsequent demodulation.

IV. Experimental Evaluation and Discussion

In this section, the test bench for experimental evaluation, the relevant data, and their analysis are provided. In order to demonstrate the feasibility of the proposed method, the process of signal modulation and demodulation is given thoroughly in this section.

A. Experimental Test Platform

In order to verify the effectiveness of the theoretical analysis, a three-phase inverter-based TPC system is established, as shown in Fig. 10. PLECS software was used to create the codes for RT BOX 1 and RT BOX 2 to control VLT three-phase two-level inverter modules. Measured currents and voltage from the voltmeter and ammeter were used for observation, control, and signal demodulation. The main experimental parameters used in this work are listed in Table I. Moreover, the process and results of demodulation are also shown in this section.

$$\begin{bmatrix} H_{d_{m=1,|n|=2}} \\ H_{q_{m=1,|n|=2}} \end{bmatrix} = -\frac{16E}{3\pi} J_2(Q_{Km}) \begin{bmatrix} \cos(\omega_0 t) & \cos(\omega_0 t - \frac{2}{3}\pi) & \cos(\omega_0 t + \frac{2}{3}\pi) \\ -\sin(\omega_0 t) & -\sin(\omega_0 t - \frac{2}{3}\pi) & -\sin(\omega_0 t + \frac{2}{3}\pi) \end{bmatrix} \begin{bmatrix} \cos(\omega_c t + \phi_c)\cos(2\omega_0 t + 2\phi_{Km}) \\ \cos(\omega_c t + \phi_c)\cos(2\omega_0 t + 2\phi_{Km} - \frac{4}{3}\pi) \\ \cos(\omega_c t + \phi_c)\cos(2\omega_0 t + 2\phi_{Km} + \frac{4}{3}\pi) \end{bmatrix}$$
$$= \begin{bmatrix} -\frac{8E}{\pi} J_2(Q_{Km})\cos(\omega_c t + \phi_c)\cos[3\omega_0 t + 2\phi_{Km}] \\ \frac{8E}{\pi} J_2(Q_{Km})\cos(\omega_c t + \phi_c)\sin[3\omega_0 t + 2\phi_{Km}] \end{bmatrix}. \quad (15)$$

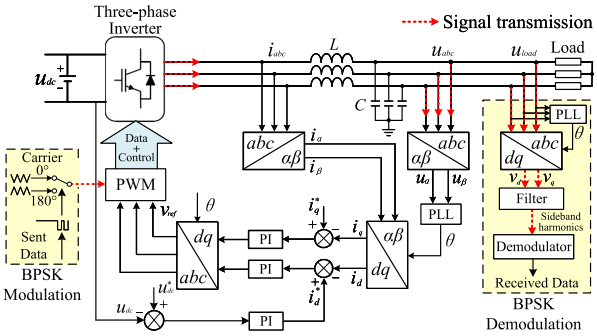

Fig. 11. Control diagram of the three-phase inverter and TPC implementation.

Although communication is the key task of this study, inverter design always plays a crucial role in power conversion, frequency synchronization, and stable power control. The scheme of the TPC three-phase inverter is shown in Fig. 11. In order to verify the generality of the method proposed in this article, the most commonly used PI control three-phase two-level inverter is selected for TPC in this work. Through appropriate parameter adjustment, stable control of the inverter output voltage and current can be realized. Meanwhile, fluctuations and oscillations can be reduced.

According to Fig. 11, there should be a controller set at the inverter side for signal modulation and a controller working at the load side for sampling and demodulation. In view of this, the RT-BOX 2 and control desk 1 worked as the inverter controller and signal modulator for TPC, while the RT-BOX 1 and control desk 2 were used for signal collection and demodulation at the load side.

B. TPC Verification

In the proposed scheme, CS modulation is used for signal modulation, and the sent digital signal is embedded into the CBPWM carrier signal by BPSK. Thus, the CBPWM process of the inverter needs to be controlled and changed in real time. Fortunately, it is practical to realize fast and real-time phase variation of the CBPWM carrier signal in PLECS software and RT BOX. The phase of the CBPWM carrier signal can vary with the transmitted signal changing. Therefore, the binary signal can be quickly embedded into the CBPWM carrier phase by BPSK modulation to achieve TPC. What is more, 0° corresponds to bit "0," and 180° corresponds to bit "1" in this article. As mentioned above, the first-order sideband harmonics with $|n| = 2$ are selected as the information medium for TPC. The modulation index M_c in the experiment is 0.85, thus $J_2(Q_{Km})$ is equal to 0.19. To extract the target sideband harmonics from the output voltage, an eighth-order bandpass filter (BPF) is designed on the receiving side. According to (4), the sideband harmonics are distributed closely and orderly around the center frequency. Thus, the center frequency of the BPF should be equal to the switching frequency (10 kHz) to extract the target sideband harmonics. For better preserving the sideband harmonics and removing the effects of other harmonics, the main parameters of the BPF are as follows: the center frequency is 10 kHz, the passband frequency range is between 8 and 12 kHz, the gain is 1 V/V (0 dB) and corner frequency attenuation is -3 dB.

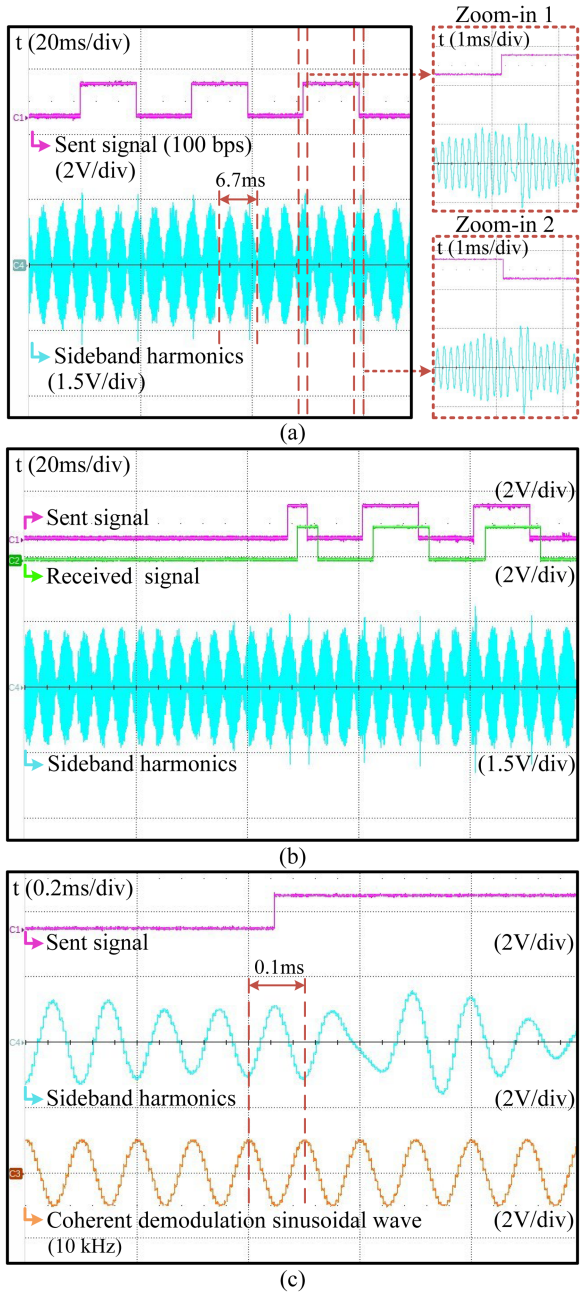

Fig. 12. BPF output harmonics. (a) Details of the sideband harmonics. (b) Comparison of sideband harmonics with and without signal transmission. (c) Sideband harmonics details and coherent demodulation sinusoidal signal.

Load side three-phase voltages were sampled by the RT Box1 every 5 μs, and an *abc*-*dq* transformation of three-phase voltages is carried out to get the target sideband harmonics under *dq*-axis. The extracted sideband harmonic from d-axis voltage is shown in Fig. 12, and details of the output harmonics with phase changes are shown in Fig. 12(a). It should be noted that the period of the envelope of output sideband harmonics is about

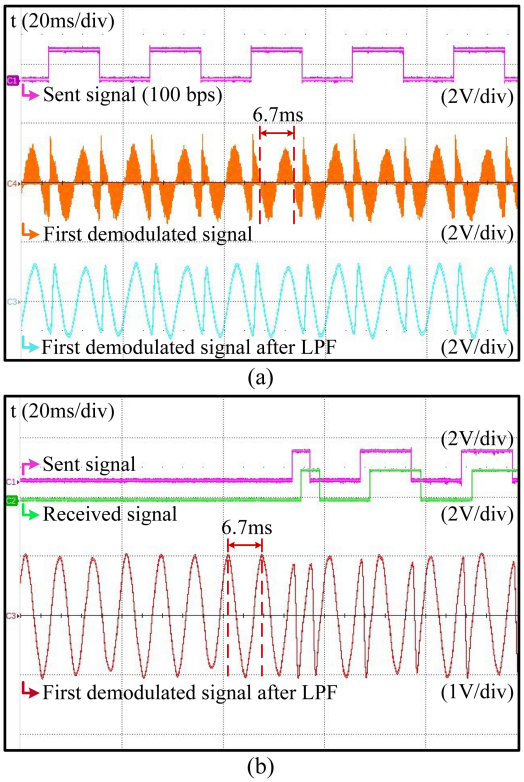

Fig. 13. First demodulation and results. (a) Coherent demodulation output signal. (b) Comparison of the demodulated signal with and without signal transmission.

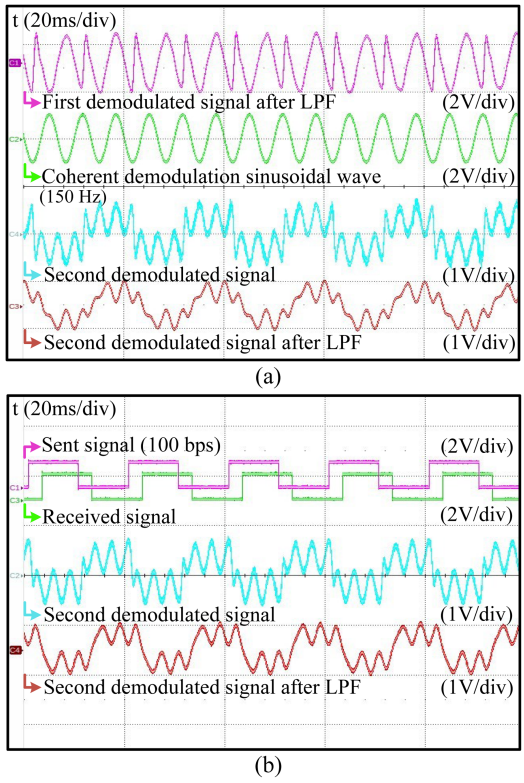

Fig. 14. Second demodulation and results. (a) Second coherent demodulation and output waveforms. (b) Received signal generated by second demodulated signal.

6.7 ms, and the frequency of the carrier signal is 10 kHz, which not only shows that the harmonics obtained by the BPF are mainly first-order sideband harmonics with $|n| = 2$, but also verifies the correctness of the formulas in (15). The waveforms of carrier DSB harmonics with and without signal transmission are presented in Fig. 12(b). Compared to the circumstances with no sent signal, little voltage disturbance would appear in the sideband harmonics when the CBPWM carrier phase changed. The value of these voltage disturbances is less than 0.5 V and can be ignored in the power system.

The first coherent demodulation results for sideband harmonics are shown in Fig. 13. In Fig. 13(a), phase changes of the demodulation signal are obvious when the transmitted signal varies. After filtering out the high-frequency components by a second-order low-pass filter (LPF), a 150 Hz sinusoidal signal is obtained, which coincides with the frequency of the second cos function in H_d in (15) ($|n| = 2$). Situations with and without signal transmission are presented clearly in Fig. 13(b). The transmitted signal is embedded into the phase changes of the LPF output demodulated signal by the first coherent demodulation. Thus, a second step of coherent demodulation is required. Here, PLL is also used to generate the sinusoidal synchronous demodulation signal (150 Hz) when the three-phase inverter works with no signal (sending bit "0").

Fig. 14 shows the details of the second coherent demodulation. It can be seen that the positivity and negativity of the second demodulated output waveform correspond to different signals.

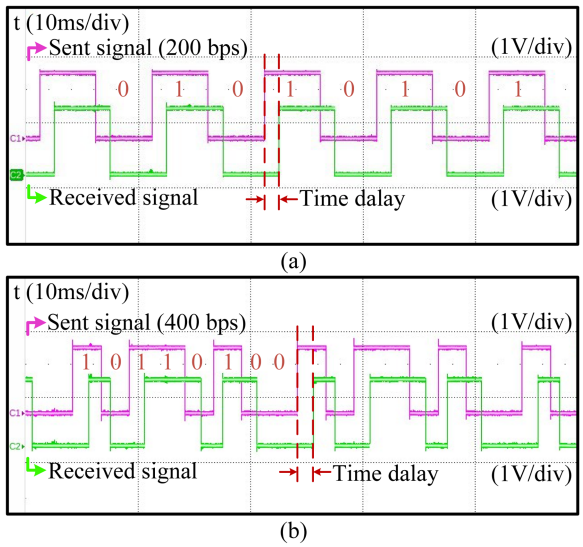

Fig. 15. Application example. (a) Transmitting binary signal "0101," transmission rate = 200 bps. (b) Transmitting binary signal "1011 0100," transmission rate = 400 bps.

Hence, the transmitted signal can be judged by comparing the positivity and negativity of the demodulated output simply. Two different application examples of the sent signal and the demodulated signal are used to prove the effectiveness of the proposed method in Fig. 15. Due to the effect of the LPF, a time delay would appear between the sent and received signal and is less than 2.5 ms, which is acceptable.

TABLE II
COMPARISON WITH THE EXISTING TPC SCHEMES IN AC POWER SYSTEMS

Reference	Application scenario	CBPWM signal modulation	Digital signal modulation	ΔTHD	Rate range
[37]	Single-phase inverters	RS modulation	DPSK	High	0–1000 bps
[23]	Cascaded multilevel inverters	CS modulation	FSK	Medium	0–600 bps
[21]	Three-phase inverters	RS modulation	/	High	0–1000 bps
[22]	Three-phase inverters	RS modulation	FSK	High	0–100 bps
[25]	Three-phase inverters	CS modulation	/	Low	0–100 bps
Proposed scheme	Three-phase inverters	CS modulation	BPSK	Low	0–400 bps

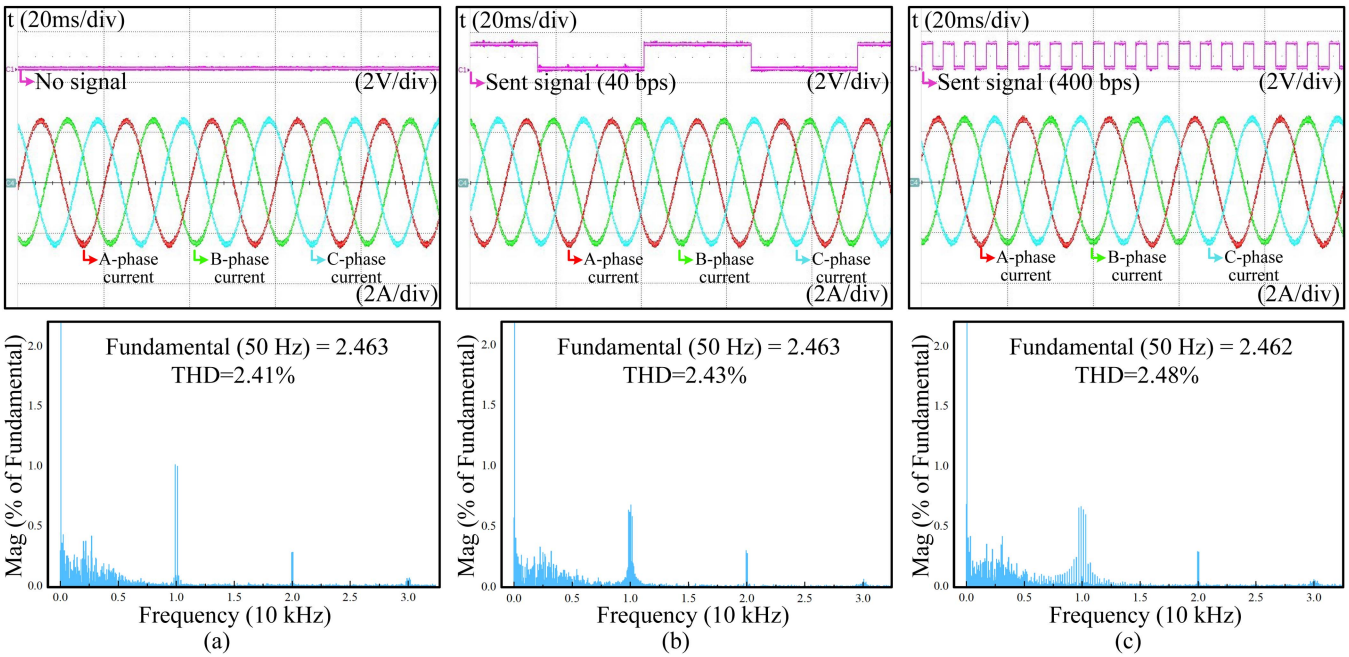

Fig. 16. Three-phase currents and FFT analysis under different Transmission rates. (a) Transmission rate = 0 bps. (b) Transmission rate = 40 bps. (c) Transmission rate = 400 bps.

C. Analysis of Current THD

Power quality represents the quantities of voltage, current, frequency, and waveform quality, which is a crucial indicator for evaluating modern power systems' stable operation and efficient performance [38]. However, due to the addition of signals, power quality would be affected inevitably. It is worth noting that the phase-changing rate of the CBPWM carrier should be less than one-tenth of the switching frequency, otherwise it will affect the CBPWM output driving signals. The recommended signaling frequency should be less than one-tenth of the switching frequency.

THD stands for the overall distortion caused by harmonics to the fundamental waveform and is an indicator used to measure the impact of all harmonics [39]. To prove the abovementioned point, Fig. 16 shows output three-phase currents and FFT analysis results under different signal transmission rates. It is noticeable that there are no carrier harmonics in the three-phase currents in this scenario, which means the sideband harmonics are more accessible information carriers for signal transmission. As for TPC, ΔTHD can be used to show the percentage change in THD caused by signal addition. Compared to the case with no signal, ΔTHD is equal to 0.02% with a 40 bps transmitted signal, and it changes into 0.08% when the rate increases to 400 bps. In other words, ΔTHD caused by CS modulation and BPSK modulation is less than 0.1%, and average THD is less than 2.5%, which indicates that the proposed TPC scheme has little impact on the output current and meets the ac grid's power quality requirements. Besides, the current disturbance caused by phase variation in Fig. 16 is about 95 mA, which has a negligible impact on power quality. The abovementioned results indicate that the proposed TPC method has good output performance of power quality-friendly characteristics.

D. Comparison With the Existing TPC Schemes in AC Power Systems

As noted above, modulation by changing the carrier frequency or superimposing the digital signal on the reference could threaten the power quality and stability from the perspective of the power system. A comparison between this method and existing TPC schemes in ac power systems is presented in Table II. According to Table II, the comparison reveals that CS modulation has less impact on ΔTHD than RS modulation, and PSK modulation is better than FSK from the power quality viewpoint. Furthermore, the proposed demodulation by abc-dq transformation and double coherent demodulation achieves a decent transmission rate in three-phase inverter applications.

V. Conclusion

In this article, a novel TPC approach for three-phase inverter-based ac power systems was presented. In the proposed method, the sideband harmonics were selected to be the signal transmission carrier for TPC in ac grid for the first time. The signal was embedded into the CBPWM carrier signal and transmitted on the power line via sideband harmonics. Compared to TPC with reference superposition and carrier frequency variation, the proposed strategy has less impact on power quality, which can be said as a power quality-friendly communication method. By double Fourier transform, harmonics with the transmitted signal can be calculated precisely. Besides, an *abc-dq* transformation for sideband harmonics is carried out to reduce the effect of carrier harmonics and increase the speed of demodulation. Finally, the feasibility of the abovementioned theory was demonstrated by the experimental platform established.

The method proposed in this article is an attempt to apply TPC in ac power systems and aims to provide a signaling strategy with less influence on power quality. In the future, this TPC method can be combined with fault diagnosis to deliver the operation of DERs to the load side or control center, contributing to the stable operation of microgrids or hybrid grids. However, there are still some issues that could be improved for inverter-based TPC systems in future work, such as the signal transmission rate improvement, long-distant TPC with low attention, anti-interference issues, and coordinated TPC between multiple inverters.

References

[1] J. Carrasco et al., "Power-electronic systems for the grid integration of renewable energy sources: A survey," *IEEE Trans. Ind. Electron.*, vol. 53, no. 4, pp. 1002–1016, Jun. 2006.

[2] J. L. Agorreta, M. Borrega, J. López, and L. Marroyo, "Modeling and control of n -paralleled grid-connected inverters with LCL filter coupled due to grid impedance in PV plants," *IEEE Trans. Power Electron.*, vol. 26, no. 3, pp. 770–785, Mar. 2011.

[3] M. T. Lawder et al., "Battery energy storage system (BESS) and battery management system (BMS) for grid-scale applications," *Proc. IEEE*, vol. 102, no. 6, pp. 1014–1030, Jun. 2014.

[4] F. Nejabatkhah, Y. W. Li, and H. Tian, "Power quality control of smart hybrid AC/DC microgrids: An overview," *IEEE Access*, vol. 7, pp. 52295–52318, 2019.

[5] J. Zhang, A. Hasandka, S. M. S. Alam, T. Elgindy, A. R. Florita, and B.-M. Hodge, "Analysis of hybrid smart grid communication network designs for distributed energy resources coordination," in *Proc. IEEE Power Energy Soc. Innov. Smart Grid Technol. Conf.*, 2019, pp. 1–5.

[6] D. Yu et al., "An incorporated power and data synchronous transmission method for SRG integrated wind power generation systems," *IEEE Trans. Ind. Electron.*, vol. 71, no. 2, pp. 1319–1327, Feb. 2024.

[7] M. Sayed, T. A. Tsiftsis, and N. Al-Dhahir, "On the diversity of hybrid narrowband-PLC/wireless communications for smart grids," *IEEE Trans. Wireless Commun.*, vol. 16, no. 7, pp. 4344–4360, Jul. 2017.

[8] A. Colak, N. Guler, and K. Ahmed, "Intelligent communication techniques for smart grid systems: A survey," in *Proc. 9th Int. Conf. Smart Grid*, 2021, pp. 273–277.

[9] H. J. Choi and J. H. Jung, "Enhanced power line communication strategy for DC microgrids using switching frequency modulation of power converters," *IEEE Trans. Power Electron.*, vol. 32, no. 6, pp. 4140–4144, Jun. 2017.

[10] N. Ginot, M. A. Mannah, C. Batard, and M. Machmoum, "Application of power line communication for data transmission over PWM network," *IEEE Trans. Smart Grid*, vol. 1, no. 2, pp. 178–185, Sep. 2010.

[11] J. Chen, J. Wu, R. Wang, R. Zhang, and X. He, "Coded PWM based switching ripple communication applied in visible light communication," *IEEE Trans. Power Electron.*, vol. 36, no. 8, pp. 9659–9667, Aug. 2021.

[12] X. He, R. Wang, J. Wu, and W. Li, "Nature of power electronics and integration of power conversion with communication for talkative power," *Nature Commun.*, vol. 11, no. 1, pp. 1–12, May 2020.

[13] S. Saggini, W. Stefanutti, P. Mattavelli, G. Garcea, and M. Ghioni, "Power line communication in DC–DC converters using switching frequency modulation," in *Proc. 21st Annu. IEEE Appl. Power Electron. Conf. Expo.*, 2006, pp. 1–6.

[14] W. Stefanutti, S. Saggini, P. Mattavelli, and M. Ghioni, "Power line communication in digitally controlled DC–DC converters using switching frequency modulation," *IEEE Trans. Ind. Electron.*, vol. 55, no. 4, pp. 1509–1518, Apr. 2008.

[15] R. Zhang, J. Wu, R. Wang, R. Yan, Y. Zhu, and X. He, "A novel battery management system architecture based on an isolated power/data multiplexing transmission bus," *IEEE Trans. Ind. Electron.*, vol. 66, no. 8, pp. 5979–5991, Aug. 2019.

[16] D. Yu et al., "A novel power and signal composite modulation approach to powerline data communication for SRM in distributed power grids," *IEEE Trans. Power Electron.*, vol. 36, no. 9, pp. 10436–10446, Sep. 2021.

[17] D. Yu, X. Wang, S. Yu, Z. Ye, T. Fernando, and H. H. C. Iu, "A soft-PWM approach to power/signal synchronous transmission for SRG-based DC microgrids," *IEEE Trans. Ind. Electron.*, vol. 67, no. 10, pp. 8450–8460, Oct. 2020.

[18] P. A. Hoeher, "FSK-based simultaneous wireless information and power transfer in inductively coupled resonant circuits exploiting frequency splitting," *IEEE Access*, vol. 7, pp. 40183–40194, 2019.

[19] J. Rodríguez, D. G. Lamar, P. F. Miaja, and J. Sebastián, "Reproducing single-carrier digital modulation schemes for VLC by controlling the first switching harmonic of the DC–DC power converter output voltage ripple," *IEEE Trans. Power Electron.*, vol. 33, no. 9, pp. 7994–8010, Sep. 2018.

[20] J. Chen, K. Liu, J. Wu, R. Wang, W. Weng, and X. He, "Simultaneous power and data transmission using combined three degrees of freedom modulation strategy in DC–DC converters," *IEEE Trans. Power Electron.*, vol. 38, no. 3, pp. 3191–3200, Mar. 2023.

[21] S. Shan and L. Umanand, "A novel fractional harmonic *d–q* domain based power line signaling technique for power converters in a microgrid," *IEEE Trans. Power Electron.*, vol. 34, no. 11, pp. 11264–11277, Nov. 2019.

[22] H. Liu, Y. Leng, and D. Yu, "Power & signal synchronous transmission strategy for three-phase voltage source inverter," in *Proc. Conf. Int. Joint Conf. Energy, Elect. Power Eng.*, 2022, pp. 145–153.

[23] Y. Zhang, G. Chen, Y. Hu, C. Gong, and Y. Wang, "Cascaded multilevel inverter based power and signal multiplex transmission for electric vehicles," *CES Trans. Elect. Mach. Syst.*, vol. 4, no. 2, pp. 123–129, 2020.

[24] M. Liserre, H. Beiranvand, Y. Leng, R. Zhu, and P. A. Hoeher, "Overview of talkative power conversion technologies," *IEEE Open J. Power Electron.*, vol. 4, pp. 67–80, 2023.

[25] Y. Leng, R. Zhu, M. Liserre, P. A. Hoeher, and H. Beiranvand, "SVPWM-based three-phase DC/AC talkative power converters," in *Proc. IECON 49th Annu. Conf. IEEE Ind. Electron. Soc.*, 2023, pp. 1–6.

[26] Q. Liu, T. Caldognetto, and S. Buso, "Review and comparison of grid-tied inverter controllers in microgrids," *IEEE Trans. Power Electron.*, vol. 35, no. 7, pp. 7624–7639, Jul. 2020.

[27] D. Yang, X. Wang, and F. Blaabjerg, "Sideband harmonic instability of paralleled inverters with asynchronous carriers," *IEEE Trans. Power Electron.*, vol. 33, no. 6, pp. 4571–4577, Jun. 2018.

[28] S. Huang, J. Xu, J. Ye, and A. Shen, "Generalized accurate harmonic calculation method based on discretized double fourier series to solve double-pulse phenomenon," *IEEE Trans. Ind. Electron.*, vol. 70, no. 6, pp. 5651–5661, Jun. 2023.

[29] R. Wang, J. Zhao, and Y. Liu, "A comprehensive investigation of four-switch three-phase voltage source inverter based on double fourier integral analysis," *IEEE Trans. Power Electron.*, vol. 26, no. 10, pp. 2774–2787, Oct. 2011.

[30] S. R. Bowes, "New sinusoidal pulsewidth-modulated inverter," *Proc. Inst. Elect. Eng.*, vol. 122, no. 11, pp. 1279–1285, Nov. 1975.

[31] D. Holmes and T. Lipo, *Pulse Width Modulation for Power Converters (Principles and Practice) (Power Engineering)*. Hoboken, NJ, USA: Wiley, 2003.

[32] W. Liang, W. Fei, and P. C.-K. Luk, "An improved sideband current harmonic model of interior PMSM drive by considering magnetic saturation and cross-coupling effects," *IEEE Trans. Ind. Electron.*, vol. 63, no. 7, pp. 4097–4104, Jul. 2016.

[33] X. Wang and F. Blaabjerg, "Harmonic stability in power electronic-based power systems: Concept, modeling, and analysis," *IEEE Trans. Smart Grid*, vol. 10, no. 3, pp. 2858–2870, May 2019.

[34] C. Wang and F. Gao, "A coherent demodulation method for short burst communication," in *Proc. IEEE 8th Joint Int. Inf. Technol. Artif. Intell. Conf.*, 2019, pp. 935–938.
[35] C. Chaichomnan, P. Khumsat, and A. Worapishet, "Single-phase, single-loop PLL-based BPSK, QPSK, 8-PSK demodulators," in *Proc. 18th Int. Conf. Electr. Eng./Electron. Comput. Telecommun. Inf. Technol.*, 2021, pp. 821–824.
[36] I. Mandourarakis, E. Koutroulis, and G. N. Karystinos, "Power line communication method for the simultaneous transmission of power and digital data by cascaded h-bridge converters," *IEEE Trans. Power Electron.*, vol. 37, no. 10, pp. 12793–12804, Oct. 2022.
[37] Y. Hui, R. Zhang, J. Wu, C. Ren, R. Wang, and X. He, "Embedding data signals into power control loop of inverters for power line communication in ac microgrids," in *Proc. 5th IEEE Conf. Energy Internet Energy Syst. Integr.*, 2021, pp. 763–767.
[38] Y. R. Li, F. Nejabatkhah, and H. Tian, *Smart Hybrid AC/DC Microgrids: Power Management, Energy Management, and Power Quality Control*. New York, NY, USA: Wiley, 2022.
[39] Y. Liu, H. Hong, and A. Q. Huang, "Real-time calculation of switching angles minimizing THD for multilevel inverters with step modulation," *IEEE Trans. Ind. Electron.*, vol. 56, no. 2, pp. 285–293, Feb. 2009.

Zewen Wang (Student Member, IEEE) was born in Shandong, China. He received the B.S. degree in automation from Jiangnan University, Wuxi, China, in 2022. He is currently working toward the M.S. degree in electronic and information engineering with the Shenzhen Institute for Advanced Study, University of Electronic Science and Technology of China, Shenzhen, China.

His research interests include communication technique in ac microgrid and power line communication.

Dehong Zhou (Senior Member, IEEE) received the B.Sc. and Ph.D. degrees in control science and engineering from the Huazhong University of Science and Technology, Wuhan, China, in 2012 and 2016, respectively.

He was a Postdoctoral Research Fellow with Nanyang Technological University, Singapore, and the University of Alberta, Edmonton, AB, Canada. Since 2020, he has been a Full Professor with the School of Automation Engineering, University of Electronic Science and Technology of China (UESTC), Chengdu, China, and Shenzhen Institute for Advanced Study, UESTC, Shenzhen, China. His research interests include power electronics and motor drives.

Xin Liu (Member, IEEE) received the B.S. degree in electrical engineering from Wuhan University, Wuhan, China, in 2015, and the Ph.D. degree in electrical engineering from Shanghai Jiao Tong University, Shanghai, China, in 2019.

From 2019 to 2021, he was with Huawei Technologies Company, Ltd., Shenzhen, China. From 2021 to 2023, he has been with the Department of Electrical Engineering, Shanghai Jiao Tong University, Shanghai, China, as a Postdoctoral Researcher. Since 2023, he joined Shenzhen Institute for Advanced Study, University of Electronic Science and Technology of China, Chengdu, China, as an Associate Researcher. His current research interests include wireless power transfer and solid-state transformers.

Zewei Shen (Member, IEEE) was born in Hubei, China. He received the B.S. degree in control science and engineering and the Ph.D. degree in electrical engineering from the Huazhong University of Science and Technology, Wuhan, China, in 2012 and 2020, respectively.

From 2020, he was a Postdoctoral Research Fellow with the School of Automation Engineering, University of Electronic Science and Technology of China (UESTC), Chengdu, China, and the Shenzhen Institute for Advanced Study, UESTC. Since 2022, he has been with the UESTC as a Lecturer. His research interests include electromagnetic interference, high-power-density power supply, and electric motor drives.

Jianxiao Zou (Member, IEEE) received the B.S., M.S., and Ph.D. degrees in control science and engineering from the University of Electronic Science and Technology of China (UESTC), Chengdu, China, in 2000, 2003, and 2009, respectively.

He is currently a Professor with UESTC, and has been the Vice Dean of Shenzhen Institute for Advanced Study, UESTC, since 2020. He was a Visiting Scholar with the University of California, Berkeley, CA, USA, in 2010; and a Senior Visiting Professor with Rutgers, the State University of New Jersey, New Brunswick, NJ, USA, in 2014. His current research interests include control theory and control engineering, renewable energy control technologies, and intelligent information processing and control.